Doppler optical coherence microscopy for studies of cochlear mechanics

Citation: Hong, Stanley S., and Dennis M. Freeman. "Doppler Optical Coherence Microscopy for Studies of Cochlear Mechanics." Journal of Biomedical Optics 11, no. 5 (2006): 054014. © 2006 SPIE

As Published: http://dx.doi.org/10.1117/1.2358702

Publisher: SPIE

Persistent URL: http://hdl.handle.net/1721.1/87598

Version: Final published version: final published article, as it appeared in a journal, conference proceedings, or other formally published context

Doppler optical coherence microscopy for studies of cochlear mechanics

Stanley S. Hong
Dennis M. Freeman
Massachusetts Institute of Technology
Research Laboratory of Electronics
Department of Electrical Engineering
and Computer Science
Cambridge, Massachusetts 02139

Abstract. The possibility of measuring subnanometer motions with micron scale spatial resolution in the intact mammalian cochlea using Doppler optical coherence microscopy (DOCM) is demonstrated. A novel DOCM system is described that uses two acousto-optic modulators to generate a stable 500-kHz heterodyne frequency. Images and motion measurements are obtained using phase-resolved analysis of the interference signal. The DOCM system permits imaging with micron-scale resolution and 85-dB sensitivity and motion measurements with 100-kHz bandwidth, directional discrimination, and 30-pm/Hz$^{0.5}$ noise floor. Images and motion measurements are presented that demonstrate the ability to resolve motions of structures of interest in a mammalian cochlea *in vitro* including the basilar membrane, reticular lamina, tectorial membrane, and outer hair cells.
 [DOI: 10.1117/1.2358702]

Keywords: biomedical optics; optical coherence tomography; motion detection; microscopy.

Paper 05211R received Aug. 1, 2005; revised manuscript received May 23, 2006; accepted for publication Jun. 22, 2006; published online Oct. 10, 2006.

1 Introduction

The mammalian auditory system can reliably detect motion of the eardrum on the order of tens of picometers and can perform spectral analysis with a quality factor ($Q_{10\ \mathrm{dB}}$) as high as 600.[1] These astonishing feats are generally attributed to an active mechanical system in the inner ear referred to as the "cochlear amplifier."[2,3] While the need for "amplification" is supported by an overwhelming body of evidence, a conclusive description of the underlying mechanisms remains elusive.

The most reliable and comprehensive studies of cochlear mechanics *in vivo* have been based on motion measurements[4–6] using heterodyne laser interferometry.[7–10] Despite the great success of studies using heterodyne laser interferometry, the interpretation of measurements obtained using this technique is confounded by a number of limitations. Artificial reflectors (e.g., glass beads) are typically required to obtain robust motion measurements. Unfortunately, the reflectors represent single-point measurements of motion on the surface of the organ of Corti, and further, it has been argued that the reflectors may not track the motion accurately.[11–13] In recent years, optical motion measurements have been obtained *in vivo* without the use of artificial reflectors.[1,14–16] However, such measurements remain restricted to the surface of the organ of Corti, while the critically important motions are believed to occur in structures within the organ itself. Recently, the resolution and sensitivity of optical coherence tomography,[17] optical coherence microscopy,[18] and corresponding optical Doppler techniques[19,20] have been shown to offer great promise for studies of both cochlear morphology[21] and cochlear mechanics.[22,23] In this paper, we present a novel Doppler optical coherence microscopy (DOCM) system that is capable of both imaging and measuring the motions of structures within the organ of Corti.

2 Experimental Apparatus

The DOCM system is based on a Michelson interferometer (Fig. 1). Spatially coherent broadband light is generated by a superluminescent diode [(SLD); center wavelength, 843 nm; full width at half maximum (FWHM) bandwidth, 52.6 nm], split by a nonpolarizing beamsplitter (BS), and detected by a single-mode fiber-coupled silicon photodetector (PD). The sample arm consists of an acousto-optic modulator [(AOM); frequency shift, 80.000 MHz] in the double-pass configuration,[24] a beam expander (BE), and an infinity-corrected 0.80–numerical-aperture (NA) water-immersion objective lens (OL). The diffraction efficiency of the AOM is 91%, and approximately 1.2 mW of optical power is incident on the sample. The reference arm consists of an AOM (frequency shift, 80.250 MHz) in the double-pass configuration, a pair of relay lenses (RLs), and a retroreflector (R). The diffraction efficiency of this AOM is nominally 12%. The RLs control the angular dispersion introduced by the AOM.

Axial scanning is accomplished by moving the OL, while transverse scanning is accomplished by moving the sample (S). The OL and retroreflector are mounted on a common single-axis translation stage to ensure that the path lengths of the interferometer arms remain matched during axial scanning.[25,26] A dichroic mirror (DM) in the sample arm permits conventional visible-light imaging with a tube lens (TL)

Address all correspondence to Dennis M. Freeman, Massachusetts Institute of Technology, Room 36-889, Cambridge, Massachusetts 02139; Tel: 617-253-8795; Fax: 617-258-5846; E-mail: freeman@mit.edu

1083-3668/2006/11(5)/054014/5/$22.00 © 2006 SPIE

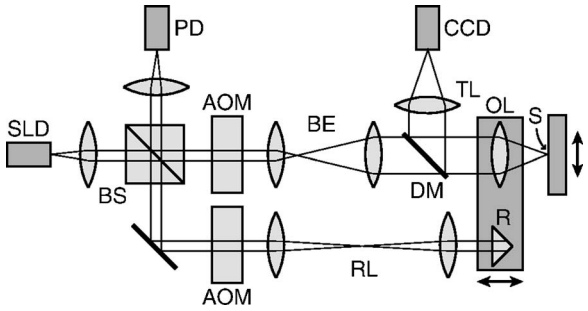

Fig. 1 Schematic diagram of the DOCM system. See text for definitions.

and a charge-coupled device (CCD) imager for initial orientation of the DOCM system to the sample.

The heterodyne frequency of the detected interference signal is 500 kHz. The 80.000-MHz and 80.250-MHz AOM drive signals are generated by two synchronized 1-GS/s digital frequency synthesizers to ensure stability of the heterodyne frequency. A 250-kHz reference signal is generated by multiplying the two drive signals using a high-isolation mixer and a low-pass filter. The photodetector and reference signals are sampled using two synchronized 5-MS/s 12-bit analog-to-digital converters and postprocessed to obtain images and motion measurements.

3 Results and Discussion

3.1 *Imaging in a Mammalian Cochlea*

The image resolution of the DOCM system is derived from both the OL and the light source. Transverse resolution is determined by the OL in a confocal imaging configuration and can be described by a transverse point-spread function[27]

$$h_{transverse}(v) = \left[\frac{2J_1(v)}{v}\right]^4, \tag{1}$$

where v is a transverse optical coordinate given by $v = (2\pi/\lambda)r\sin(\mathrm{NA})$ and J_1 is a Bessel function of the first kind. In contrast, axial resolution is determined by both the OL and the coherence properties of the light source. The axial resolution of the OL can be described by an axial point-spread function[27]

$$h_{axial}(u) = \left[\frac{\sin(u/4)}{u/4}\right]^4, \tag{2}$$

where u is an axial optical coordinate given by $u = (8\pi/\lambda)z\sin^2(\mathrm{NA}/2)$. If the confocal gate and coherence gate are aligned and scanned in synchrony (achieved in the DOCM system by mounting the OL and retroreflector on a common translation stage), the interferometric term in the detector current can be written as[28]

$$\tilde{i}_d(l_r) \propto \int_0^\infty \sqrt{R_s(l_s)h_{axial}(l_r - l_s)}R_{ii}(l_r - l_s)dl_s, \tag{3}$$

where l_r and l_s denote, respectively, the reference and sample arm lengths; R_s is the reflectivity of the sample; and R_{ij} is the source autocorrelation function. The response of the DOCM system to a point scatterer can be written as a simple product

$$\tilde{i}_d(l_r) \propto \sqrt{h_{axial}(l_r)}R_{ii}(l_r). \tag{4}$$

Note that with a low NA OL, axial resolution is determined almost entirely by the coherence length of the light source.

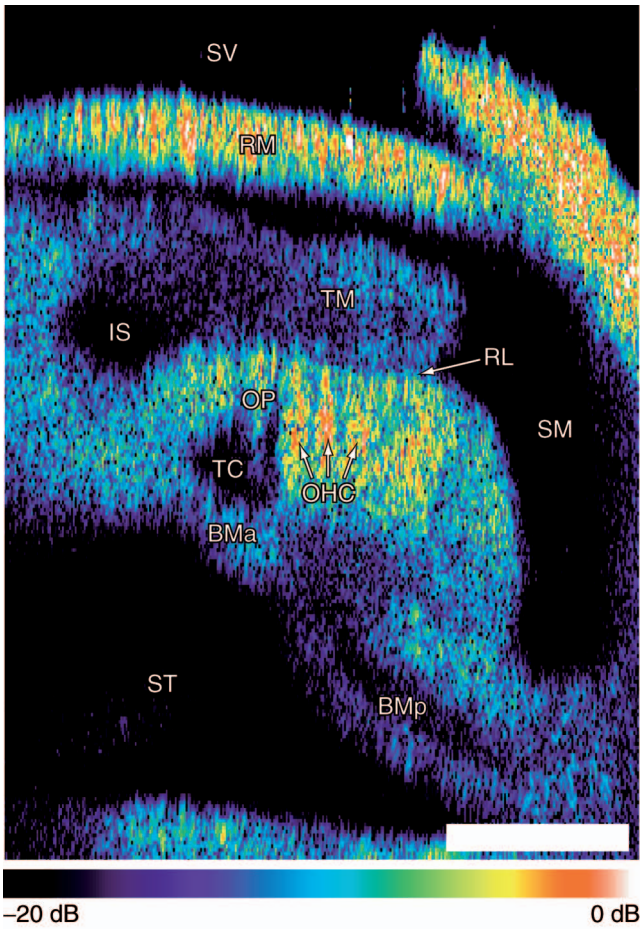

Fig. 2 Image of an isolated gerbil cochlea obtained using DOCM. The pixel size is 1×2 μm. The scale bar is 100 μm.

Figure 2 shows the cochlea of a Mongolian gerbil (*Meriones unguiculatus*) imaged using the DOCM system. The cochlea was isolated and fixed in an artificial perilymph solution[29] containing 2.5% glutaraldehyde. The apical turn was opened by removing the bony wall enclosing scala vestibuli using the tip of a scalpel. The image shows a cross section of the exposed apical turn. Light from the DOCM system is incident from the top; the cochlear partition is imaged through Reissner's membrane. The central axis of the cochlea is tilted approximately 30 deg relative to the optical axis. Backscattered intensity is shown on a logarithmic scale in order to display a wide dynamic range.

Although the DOCM image in Fig. 2 is degraded by speckle noise, numerous features relevant to cochlear mechanics are readily identified including the fluid spaces scala vestibuli (SV), scala media (SM), and scala tympani (ST) as well as the inner sulcus (IS) and tunnel of Corti (TC), Reiss-

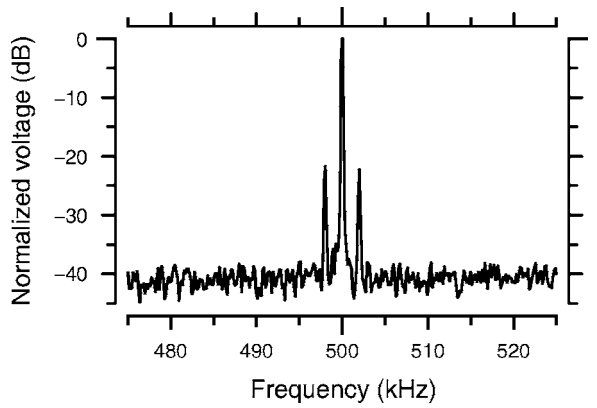

Fig. 3 Spectrum of photodetector signal with DOCM beam focused on top of first OHC. The optical heterodyne frequency is 500 kHz, and the stimulus frequency is 2.0 kHz.

ner's membrane (RM), the tectorial membrane (TM), the reticular lamina (RL), the arcuate and pectinate zones of the basilar membrane (BMa and BMp, respectively), an outer pillar (OP) cell, and three outer hair cells (OHCs). The integrity of the sample was verified by subsequent conventional visible-light imaging. The most strongly backscattering structures in the cochlear partition are the OHCs. Note that the region beneath the OHCs appears shadowed. The apparent increased thickness of RM in Fig. 2 is an artifact due to the high reflectivity of the membrane and the normalization of the logarithmic scale. The FWHM thickness of RM in Fig. 2 is approximately 12 μm.

3.2 *Measuring Motion in a Mammalian Cochlea*

Motion of the sample can be measured using the DOCM system by monitoring the difference in optical path length between the sample and reference arms. In Doppler optical coherence tomography, this can be achieved by monitoring the instantaneous phase of the heterodyne signal using a Hilbert transform.[30] In the DOCM system, the difference in instantaneous phase $\phi(n)$ between the heterodyne signal $V_{het}(n)$ and reference signal $V_{ref}(n)$ can be estimated accordingly as

$$\phi(n) = \tan^{-1}\left(\frac{H[V_{het}(n)]}{V_{het}(n)}\right) - 2\tan^{-1}\left(\frac{H[V_{ref}(n)]}{V_{ref}(n)}\right), \quad (5)$$

where H denotes the discrete Hilbert transform. Sample displacement $d(n)$ along the optical axis can be estimated from $\phi(n)$ as

$$d(n) = \frac{1}{2k\tilde{n}}\phi(n), \quad (6)$$

where $k=2\pi/\lambda$ and $\tilde{n}$ is the refractive index.

The sample shown in Fig. 2 was mechanically stimulated using a piezoelectric transducer (nominal unloaded resonant frequency, 261 kHz) attached to the sample mount. The transducer was driven at 2.0 kHz. Motion artifacts are not apparent in Fig. 2 due to the low amplitude of the motions (tens of nanometers). However, motion is readily detected in the spectrum of the heterodyne signal. For example, Fig. 3 shows the spectrum of the heterodyne signal measured at the top of the first OHC. The plot shows the magnitude of the 32,768-point discrete Fourier transform of $V_{het}(n)$ (corresponding to a 6.6-ms measurement time). For clarity, 10 measurements were averaged to reduce the spectral noise variance. Note that the amplitude of the 500-kHz peak in Fig. 3 corresponds to the brightness of 1 pixel in Fig. 2, while the amplitude and phase of the 500±2-kHz side peaks correspond respectively to the amplitude and phase of motion measured at that pixel. Every pixel in Fig. 2 similarly represents a simultaneous measurement of backscattered intensity and motion.

Table 1 Motion of cochlear structures measured with DOCM.

Location	Amplitude (nm)	Phase (rad)[a]
OHC1 (top)	15.8±1.9	−0.08±0.09
OHC1 (bottom)	16.2±1.4	−0.07±0.09
OHC2 (top)	15.2±1.6	−0.10±0.12
OHC2 (bottom)	15.2±1.3	−0.10±0.07
OHC3 (top)	14.6±1.4	−0.15±0.13
OHC3 (bottom)	15.0±1.1	−0.15±0.07
BMa	15.8±3.8	−0.01±0.20
BMp	15.7±2.6	−0.19±0.21
TM	12.7±3.5	−0.28±0.27
RM	17.1±1.1	0.02±0.04
Bone	17.4±1.1	0.00±0.04

[a]Phase measurements are referenced to the stimulus.

Table 1 shows the measured motion at several locations in Fig. 2. The motion measurements were generated by calculating the displacement $d(n)$ at each pixel in the 10×10 pixel region centered at the location of interest. Displacement signals corresponding to low-intensity pixels contained phase wrapping errors and were subsequently disregarded. The displacement signals were least-squares fit to 2.0-kHz sinusoids, and Table 1 shows the means and standard deviations of the fit amplitudes and phases. Note that the coherence length of the SLD (4.5 μm in water) is sufficiently short to differentiate the motion of the top and the bottom of each OHC, regardless of the NA of the OL. Also, the DOCM system is sufficiently sensitive to measure the motions of weakly backscattering structures such as the TM. Note that in contrast to stapes-driven acoustic stimulation, mechanical stimulation does not create a pressure differential across the cochlear partition. Consequently, large relative motions are not expected in Table 1.

The motion measurement accuracy of the DOCM system was compared with that of a commercial laser Doppler vibrometer system (nominal accuracy, 1%) by measuring the motion of a cover slip mounted on a piezoelectric actuator. The actuator was driven at 100 Hz. Simultaneous measurements using the two systems agreed to within 3% in amplitude and 0.04 rad in phase.

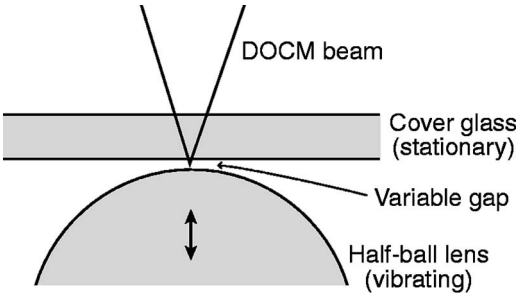

Fig. 4 Experimental setup for examining axial resolution of motion measurement.

The ability to discriminate motions at different depths was examined by measuring the motions of two glass/water interfaces separated by a variable gap; the first interface was stationary, while the second interface was mechanically driven. As illustrated in Fig. 4, the bottom surface of a microscope cover glass served as the first interface, while the top surface of an uncoated half-ball lens (radius, 1 mm) served as the second interface. The half-ball lens was attached to a piezoelectric transducer (nominal unloaded resonant frequency, 261 kHz) driven at 2.0 kHz. The use of a ball lens allowed the two interfaces to come in close proximity without contact. Scattering medium was not simulated as direct line of sight to the organ of Corti is prerequisite to most studies of cochlear mechanics and the fluid spaces in the cochlea are optically transparent. Figure 5 shows the motion of the two interfaces measured using the DOCM system as the size of the gap was varied from 100 to 0 μm. The results show that the motions of the two interfaces are clearly resolved with a separation of more than 10 μm and difficult to differentiate with a separation of less than 3 μm.

The noise characteristics of the DOCM system were examined by imaging and measuring the motion of a stationary mirror with a neutral density filter (optical density, 3) inserted in the sample arm between the OL and the DM. The measured imaging sensitivity of the DOCM system is approximately 85 dB. Figure 6 shows the magnitude of the 32,768-point

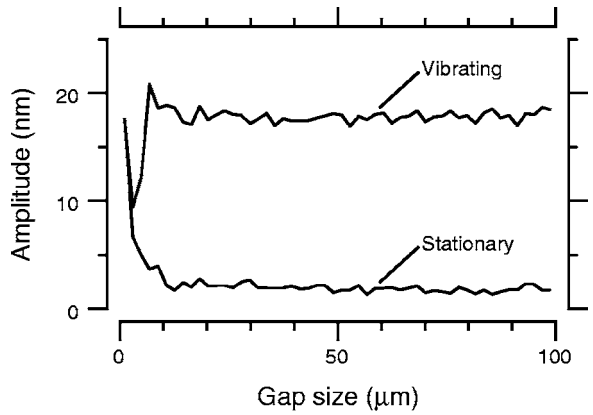

Fig. 5 Motion of vibrating and stationary interfaces measured with DOCM. The vibrating and stationary interfaces are the top surface of the half-ball lens and the bottom surface of the cover glass shown in Fig. 4, respectively.

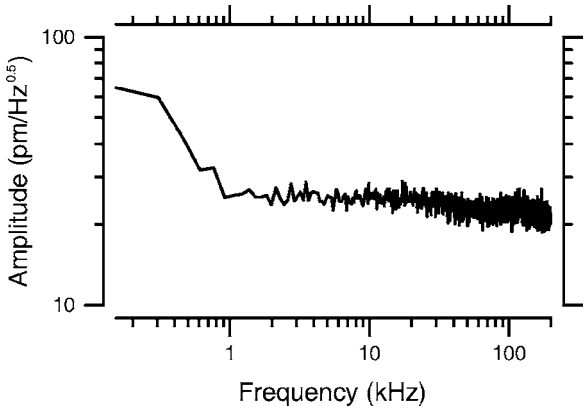

Fig. 6 Noise floor of motion measurement with sample reflectivity of 10^{-6}.

discrete Fourier transform of $d(n)$ (corresponding to a 150-Hz measurement bandwidth). One hundred measurements were averaged to reduce the spectral noise variance. With a sample reflectivity of 10^{-6} (which is comparable to the reflectivities of structures within the organ of Corti[31]), the motion measurement noise floor is less than 30 pm/Hz$^{0.5}$ at frequencies above 1 kHz. The motion amplitude of the basilar membrane is on the order of 100 pm at the threshold of hearing,[3] and the upper limit on the frequency range of hearing is between 10 and 100 kHz for most mammals.

The optical access requirements of DOCM are identical to those of heterodyne laser interferometry. Consequently, the technique is expected to find immediate application in both *in vitro* and *in vivo* studies of hearing. In a clinical setting, DOCM could be used to measure the motions of outer- and middle-ear structures to diagnose disorders such as otosclerosis. In a research setting, DOCM could clarify the relation between OHC somatic motility[32] and the sharpness of cochlear tuning, one of the largest unresolved issues in cochlear mechanics.

4 Summary

We have presented a novel DOCM system and have obtained images and motion measurements of structures within the organ of Corti of a mammalian cochlea *in vitro*. We believe the system is ideal for use in both *in vitro* and *in vivo* studies of cochlear mechanics and, more generally, in applications where low sample reflectivity and restricted NA impede optical measurement of motion.

Acknowledgments

The authors wish to acknowledge Tony Ko, A. J. Aranyosi, Scott Page, Kinu Masaki, Joseph Kovac, and Annie Chan for their contributions. All animal procedures were approved by the Massachusetts Institute of Technology Committee on Animal Care. This work was supported by the National Institutes of Health under Grant No. 1-R21-DC007111-01.

References

1. M. Kössl and I. J. Russell, "Basilar membrane resonance in the cochlea of the mustached bat," *Proc. Natl. Acad. Sci. U.S.A.* **92**, 276–279 (1995).

2. P. Dallos, "The active cochlea," *J. Neurosci.* **12**, 4575–4585 (1992).
3. L. Robles and M. A. Ruggero, "Mechanics of the mammalian cochlea," *Physiol. Rev.* **81**, 1305 (2001).
4. A. L. Nuttall, D. F. Dolan, and G. Avinash, "Laser Doppler velocimetry of basilar membrane vibration," *Hear. Res.* **51**, 203–213 (1991).
5. M. A. Ruggero and N. C. Rich, "Application of a commercially-manufactured Doppler-shift laser velocimeter to the measurement of basilar-membrane vibration," *Hear. Res.* **51**, 215–230 (1991).
6. N. P. Cooper and W. S. Rhode, "Basilar membrane mechanics in the hook region of cat and guinea-pig cochleae: Sharp tuning and nonlinearity in the absence of baseline position shifts," *Hear. Res.* **63**, 163–190 (1992).
7. Y. Yeh and H. Z. Cummins, "Localized fluid flow measurements with an He-Ne laser spectrometer," *Appl. Phys. Lett.* **4**, 176–178 (1964).
8. W. H. Stevenson, "Optical frequency shifting by means of a rotating diffraction grating," *Appl. Opt.* **9**, 649–652 (1970).
9. L. E. Drain, *The Laser Doppler Technique*, Wiley, New York (1986).
10. J.-F. Willemin, R. Dändliker, and S. M. Khanna, "Heterodyne interferometer for submicroscopic vibration measurements in the ear," *J. Opt. Soc. Am. A* **83**, 787–795 (1988).
11. P. M. Sellick, G. K. Yates, and R. Patuzzi, "The influence of Mossbauer source size and position on phase and amplitude measurements of the guinea pig basilar membrane," *Hear. Res.* **10**, 101 (1983).
12. S. M. Khanna, M. Ulfendahl, and C. R. Steele, "Vibration of reflective beads placed on the basilar membrane," *Hear. Res.* **116**, 71–85 (1998).
13. N. P. Cooper, "Vibration of beads placed on the basilar membrane in the basal turn of the cochlea," *J. Opt. Soc. Am. A* **106**, L59–L67 (1999).
14. N. P. Cooper, "An improved heterodyne laser interferometer for use in studies of cochlear mechanics," *J. Neurosci. Methods* **88**, 93–102 (1999).
15. S. M. Khanna and L. F. Hao, "Reticular lamina vibrations in the apical turn of a living guinea pig cochlea," *Hear. Res.* **132**, 15–33 (1999).
16. T. Ren, "Longitudinal pattern of basilar membrane vibration in the sensitive cochlea," *Proc. Natl. Acad. Sci. U.S.A.* **99**, 17101–17106 (2002).
17. D. Huang, E. A. Swanson, C. P. Lin, J. S. Schuman, W. G. Stinson, W. Chang, M. R. Hee, T. Flotte, K. Gregory, C. A. Puliafito, and J. G. Fujimoto, "Optical coherence tomography," *Science* **254**, 1178–1181 (1991).
18. J. A. Izatt, M. R. Hee, G. M. Owen, E. A. Swanson, and J. G. Fujimoto, "Optical coherence microscopy in scattering media," *Opt. Lett.* **19**, 590–592 (1994).
19. X. J. Wang, T. E. Milner, and J. S. Nelson, "Characterization of fluid flow velocity by optical Doppler tomography," *Opt. Lett.* **20**, 1337–1339 (1995).
20. T. E. Milner, S. Yazdanfar, A. M. Rollins, J. A. Izatt, T. Lindmo, Z. Chen, J. S. Nelson, and X.-J. Wang, "Doppler optical coherence tomography," in *Handbook of Optical Coherence Tomography*, B. E. Bouma and G. J. Tearney, Eds., pp. 203–236, Marcel Dekker, New York (2002).
21. B. J. F. Wong, J. F. de Boer, B. Y. Park, Z. Chen, and J. S. Nelson, "Optical coherence tomography of the rat cochlea," *J. Biomed. Opt.* **5**, 367–370 (2000).
22. S. Matthews, E. Porsov, and A. L. Nuttall, "Some geometrical aspects of cochlear interferometry," presented at the Association for Research in Otolaryngology Twenty-Sixth Annual Midwinter Research Meeting, Daytona Beach, Florida, 22–27 February (2003).
23. S. L. Jacques, S. Matthews, G. Song, and A. L. Nuttal, "Optical coherence tomography of the organ of Corti," presented at the Association for Research in Otolaryngology Twenty-Eighth Annual Midwinter Research Meeting, New Orleans, Louisiana, 19–24 February (2005).
24. H.-W. Wang, A. M. Rollins, and J. A. Izatt, "High speed, full field optical coherence microscopy," in Coherence Domain Optical Methods in Biomedical Science and Clinical Applications III, V. V. Tuchin and J. A. Izatt, Eds., *Proc. SPIE* **3598**, 204–212 (1999).
25. J. M. Schmitt, S. L. Lee, and K. M. Yung, "An optical coherence microscope with enhanced resolving power in thick tissue," *Opt. Commun.* **142**, 203–207 (1997).
26. F. Lexer, C. K. Hitzenberger, W. Drexler, S. Molebny, H. Sattmann, M. Stricker, and A. F. Fercher, "Dynamic coherence focus OCT with depth-independent transversal resolution," *J. Mod. Opt.* **46**, 541–553 (1999).
27. M. Gu, C. J. R. Sheppard, and X. Gan, "Image formation in a fiber-optical confocal scanning microscopy," *J. Opt. Soc. Am. A* **8**, 1755–1761 (1991).
28. H.-S. Wang, J. A. Izatt, and M. D. Kulkarni, "Optical coherence microscopy," in *Handbook of Optical Coherence Tomography*, B. E. Bouma and G. J. Tearney, Eds., pp. 275–298, Marcel Dekker, New York (2002).
29. D. M. Freeman, D. K. Hendrix, D. Shah, L. F. Fan, and T. F. Weiss, "Effect of lymph composition on an in vitro preparation of the alligator lizard cochlea," *Hear. Res.* **65**, 83–98 (1993).
30. Y. Zhao, Z. Chen, C. Saxer, S. Xiang, J. F. de Boer, and J. S. Nelson, "Phase-resolved optical coherence tomography and optical Doppler tomography for imaging blood flow in human skin with fast scanning speed and high velocity sensitivity," *Opt. Lett.* **25**, 114–116 (2000).
31. S. M. Khanna, J.-F. Willemin, and M. Ulfendahl, "Measurement of optical reflectivities in cells of the inner ear," *Acta Oto-Laryngol., Suppl.* **467**, 69–75 (1989).
32. W. E. Brownell, C. R. Bader, D. Bertrand, and Y. de Ribaupierre, "Evoked mechanical responses of isolated cochlear outer hair cells," *Science* **227**, 194–196 (1985).